Enhanced Optical Properties of ZnO-TiO_2 Films Through Co-Sensitization with Multiple Natural Dyes

Musyarofah Musyarofah[1*], Inas Nuraini[1], Budi Prayitno[2], Lusi Ernawati[3], Andi Idhil Ismail[4], and Triwikantoro Triwikantoro[5]

[1]*Department of Physics, Institut Teknologi Kalimantan, Jl. Soekarno-Hatta Km. 15, Balikpapan 76127, Indonesia*

[2]*Department of Mechanical Engineering, Universitas Balikpapan, Jl. Pupuk Raya, Balikpapan 76114, Indonesia*

[3]*Department of Chemical Engineering, Institut Teknologi Kalimantan, Jl. Soekarno-Hatta Km. 15, Balikpapan 76127, Indonesia*

[4]*Department of Mechanical Engineering, Institut Teknologi Kalimantan, Jl. Soekarno-Hatta Km. 15, Balikpapan 76127, Indonesia*

[5]*Department of Physics, Faculty of Data Science and Analytics, Institut Teknologi Sepuluh Nopember, Kampus ITS Sukolilo, Surabaya 60111, Indonesia*

* ***Corresponding author:***

email: musyarofah@lecturer.itk.ac.id

Received: May 14, 2024
Accepted: November 13, 2024

DOI: 10.22146/ijc.96154

Abstract: *The ZnO-TiO_2 films were co-sensitized with single, double, and triple natural dyes, leading to distinct effects on the optical properties. ZnO (wurtzite) and TiO_2 (anatase) were prepared from commercial powders and the XRD results revealed that the crystallite size is 158 and 443 nm, respectively. The UV absorbance of ZnO powder shows significant peaks at wavelengths of 255 and 345 nm, with a band gap energy of 3.07 eV. Meanwhile, TiO_2 powder exhibits a maximum peak at 325 nm and possesses a band gap energy of 3.16 eV. The extraction of natural dyes (*Moringa oleifera, Biancaea sappan, Matricaria chamomilla, Rosa, *and* Chrysanthemum*) was carried out using a cost-effective and simple method involving immersion in ethanol for 2 × 24 h followed by filtration. FTIR test results show the presence of O–H, C–H, C=C, and C–O functional groups. The results of coating the ZnO-TiO_2 film with natural dyes show that the UV spectrum peaks are higher than the visible light wavelength. Co-sensitization of double natural dyes demonstrated different effects on the ZnO-TiO_2 film, i.e., achieved panchromatic absorption mainly in the UV wavelength spectrum.*

Keywords: *photoanode; absorbance; optical properties; co-sensitized; ZnO-TiO_2*

■ INTRODUCTION

To carry out human's daily activities, energy is an essential necessity. Fossil fuels, for example, are a non-renewable energy sources that are frequently used, which has an impact on their supply. Furthermore, environmentalists recommend reducing the reliance on fossil fuels because of their detrimental impact on climate change [1]. On the other side, the sun offers a source of clean energy that has a lot of potential to be harnessed through innovations like dye-sensitized solar cells (DSSCs). Due to its low cost and simple manufacturing procedures, DSSC technology has attracted attention [2]. The semiconductor-coated photoanode, sensitizer, cathode, and electrolyte are the core components of DSSCs, and ongoing research strives to improve them for optimum efficiency, durability, and cost reduction.

The role of the sensitizer is to capture sunlight and convert it into electrical energy. In previous research, inorganic ruthenium was used as a sensitizer, achieving DSSC energy conversion efficiency of up to 13% [3-5]. However, the cost of these materials is high and their natural availability is limited [6]. On the other hand, natural dyes can be obtained from plant components such as flowers, leaves or stems, which contain pigments that give them color. These dyes, involved in photon absorption, significantly impact the efficiency of DSSC

technology. The ability to capture sunlight depends on the absorption properties of the dye.

Most of the semiconductor materials used are derived from TiO_2, which has a band gap energy between 3.2 and 3.8 eV [7]. Some researchers combine two to three semiconductor materials, called composites, to improve the properties of the semiconductor material. ZnO stands out as a semiconductor with favorable properties that enhance the photocatalytic activity of TiO_2. ZnO has a wider band gap energy (about 3.37 eV) [8]. Mixing ZnO with TiO_2 is expected to enhance the ability to capture sunlight effectively. This involves mixing TiO_2 powder with ZnO in a mass ratio of 1:3 ZnO in TiO_2, both of commercial origin. These two powders exhibit distinct crystal structures and phase properties that influence their optical and electrical properties. In addition, ZnO and TiO_2 have different morphologies that can affect the performance of both powders.

Natural dye extracts and semiconductor powders serve as basic materials for fabricating anodes in DSSCs. In addition to improvements in sensitizers and semiconductors, the performance of DSSCs can also be improved through dye co-sensitization. This co-sensitization is performed to achieve broad-spectrum light absorption, thereby optimizing sunlight absorption. This process involves combining two or three different dyes. This study aims to investigate the impact of dye co-sensitization on the optical properties of ZnO-TiO_2 films synthesized using the spin coating method. Combining one, two, or three different natural dyes aims to achieve broad-spectrum light absorption and optimize sunlight absorption. The study involves detailed characterization of the films using XRD, SEM, UV-vis, and FTIR spectroscopy to understand the effects of dye co-sensitization on the optical properties of the natural dye-coated ZnO-TiO_2 films.

■ EXPERIMENTAL SECTION

Materials

The raw materials for natural dyes were *Moringa oleifera* leaves, *Biancaea sappan* leaves, *Matricaria chamomilla* flowers, *Rosa* flowers, and *Chrysanthemum* flowers. The solvent used for the dye maceration process was ethanol (Merck, 99.9%). ZnO-TiO_2 composite was prepared from commercial powders (Merck, purity of 99 and 98%, respectively).

Instrumentation

Characterization using XRD (Bruker D8 Advance) was carried out to identify the crystal structure and phase composition of the material. This measurement was carried out at the angle of at $2\theta = 10–70°$ with the Cu-Kα target ($\lambda_1 = 1.54060$ Å; $\lambda_2 = 1.54443$ Å). Qualitative analysis was carried out using *Match!* software to identify the phase. Meanwhile, quantitative analysis was performed using Rietica software and the Rietveld method to determine the phase composition and lattice parameters [9-10]. *MAUD* software was used to estimate the crystallite size. The microstructure of the powders was examined using Phenom Pro-x SEM at 15 kV. FTIR data were collected for the 500 to 4000 cm^{-1} wavenumbers using a Bruker Vertex7.0v FTIR spectrometer to characterize the interatomic bonding states through the vibration spectra. The optical characteristics of the films, particularly the absorption in the UV and visible light wavelength range (400–700 nm), were investigated using an Analytic Jena Specord 200 Plus UV-vis spectrophotometer.

Procedure

Synthesis of photoanode film procedures

The extraction of the natural dyes was conducted using a solvent extraction technique called maceration [11]. This process involves grinding the raw materials into a powder weighing about 2 g, then soaking them in 20 mL of ethanol for 48 h, and storing in an environment protected from light and at room temperature. The natural pigment extract is then concentrated to separate the ethanol from the pigment through distillation. This involves heating the extract to 78.5 °C for 60 min. Ethanol evaporates and condenses back to a liquid state collected in a container. This results a more concentrated extract than the original extract. Among the five natural dyes extracted, three dyes were selected to coat the ZnO-TiO_2 film. ZnO-TiO_2 composite was prepared from commercial powders with a weight ratio 1:3 by physical mixing using mortar for

30 min. Then, the ZnO-TiO_2 film was fabricated by combining ZnO-TiO_2 powder and dye solution at a ratio of 0.5 g/2 mL, then mixed for 10 min. The resulting solution was then applied to the ITO glass surface using the spin coating method and then heated at 100 °C for 10 min.

■ RESULTS AND DISCUSSION

The results obtained from UV-vis spectrophotometry, shown in Fig. 1, indicate that all five dyes exhibit light absorption in the visible spectrum, especially in the wavelength range from 400 to 700 nm. Each dye extract has specific wavelengths where it absorbs light most strongly, known as absorption peaks. These peaks are indicative of the presence of particular pigments in the dye. The heights of these absorption peaks are compared. Larger peaks indicate higher concentrations of absorbing pigments, suggesting that these dyes are more effective at absorbing light. The range of wavelengths over which each dye absorbs light is considered. Dyes with broader absorption ranges are often more versatile and effective. The concentration of pigments in the dye extracts is inferred from the intensity of the absorption peaks. A higher concentration means a stronger dye. The evaluation may also involve comparing the results with previous research to ensure consistency and validate findings. For example, the peaks observed for *M. oleifera* at specific wavelengths (663 nm for chlorophyll-a, 647 nm for chlorophyll-b, and 470 nm for carotenoids) are consistent with known absorption characteristics of these pigments [12]. Similarly, *B. sappan* showed a dominant peak in the 450–500 nm range, consistent with the findings of Nurlinda et al. [13]. *M. chamomilla*, with a dominant peak spanning from 450 to 700 nm, is consistent with the absorption peak reported in the study of Mansour et al. [14], who recorded the absorbance of *M. chamomilla* at wavelengths from 365 to 515 nm. In this specific case, *M. oleifera*, *B. sappan*, and *M. chamomilla* were identified as the main dyes of interest because their absorption peaks were larger and spanned significant portions of the visible spectrum compared to *Rosa* and *Chrysanthemum*. For instance, *M. oleifera* showed a broad absorption range from 450 to 600 nm with a significant

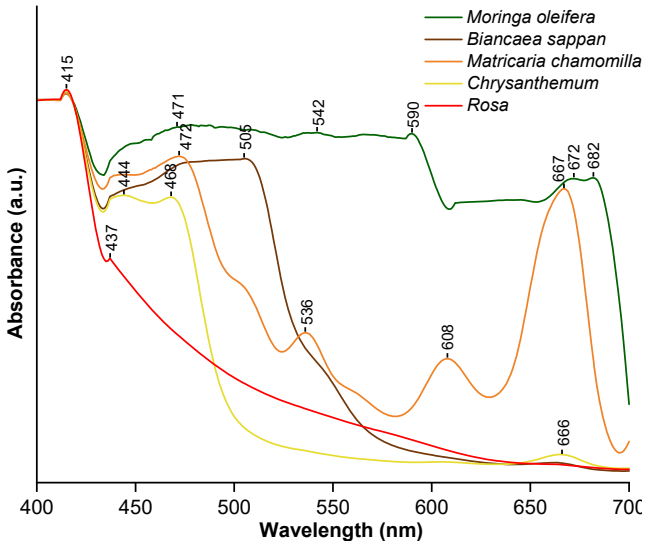

Fig 1. UV-vis absorption spectra of *M. oleifera*, B. *sappan*, *M. chamomilla*, *Rosa*, and *Chrysanthemum* extract

peak at 590 nm, indicating a high concentration of pigments capable of effectively absorbing light in this range. By focusing on these dyes with substantial absorption contributions, we ensure that the selected dyes are the most effective for their intended use, providing the desired optical properties.

Additionally, *M. oleifera*, *B. sappan*, *M. chamomilla*, *Rosa*, and *Chrysanthemum* underwent FTIR analysis to evaluate the composition of functional groups or compounds in the colored extract. As shown in Fig. 2, natural dye extracts exhibited significant peaks at specific wavenumbers: 3600–3200 cm^{-1}, indicating the presence of O–H functional groups (bonded to alcohol, phenol, and hydroxyl); 2980–2970 cm^{-1}, indicates C–H functional group (typical of alkanes and hydrocarbons); 1680–1610 cm^{-1}, representing the functional group C=C (characteristic of alkenes); and 1300–1050 cm^{-1}, representing the C–O functional group (bonded to alcohols, ethers, carboxylic acids, and esters). These results show that the natural dye was extracted using ethanol as a solvent, with functional group analysis showing the presence of O–H, C–H, C=C and C–O.

B. sappan contains the color pigment Brazilin, which belongs to the group of flavonoid compounds [13]. These compounds are polar because they have a O–H group, allowing them to be soluble in ethanol [15-16].

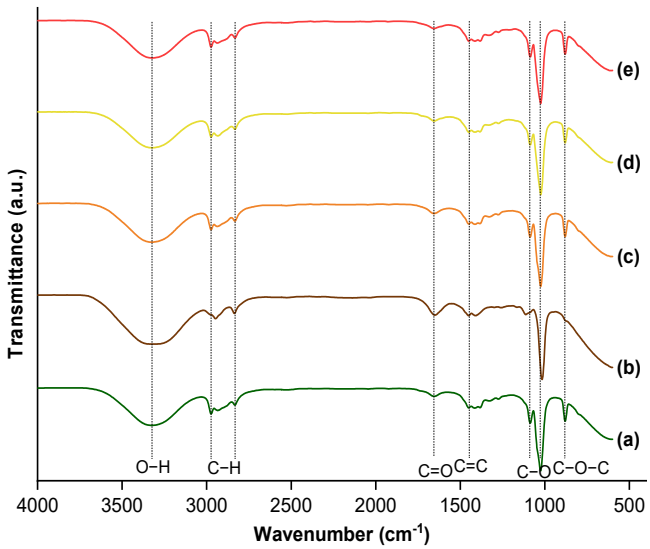

Fig 2. FTIR spectra of natural dyes extract (a) *M. oleifera*, (b) *B. sappan*, (c) *M. chamomilla*, (d) *Chrysanthemum*, and (e) *Rosa*

Fig. 3 shows the molecular structure of Brazilin, which contribute to the FTIR absorption bands, particularly O–H stretching and C=C aromatic ring stretching. *M. oleifera* extract gives a green color, indicating chlorophyll pigment. This is consistent with the FTIR data of *M. oleifera*, which shows peaks in the range 3600–3200 cm^{-1} and exhibits asymmetric fluctuations of hydrogen in the porphyrin ring [17]. Porphyrins are compounds that create green pigments called chlorophyll [18]. Fig. 3 provides the molecular structure of chlorophyll-a, highlighting the porphyrin ring with a central magnesium ion and the phytol tail. This aids in understanding the characteristic FTIR peaks such as C=O stretching, N–H bending, and C–H stretching vibrations. However, a closer look at the FTIR plot of *M. oleifera* in Fig. 2 shows several small peaks, indicating the presence of organic molecular compounds from complex groups in the extract. This observation is consistent with the previous study [19], which also detected small peaks in their extraction analysis. The principal components in *M. chamomilla* extracts are flavonoids, such as apigenin. Fig. 3 shows the molecular structure of apigenin, showing its aromatic rings and O–H groups that are responsible for specific FTIR peaks. The main constituents of *Rosa* extracts are anthocyanins, particularly cyanidin-3-glucoside. Fig. 3 presents the molecular structure of cyanidin-3-glucoside, which are relevant to the FTIR spectra interpretation, particularly in the O–H and C=O stretching regions. The primary pigments in *Chrysanthemum* are flavonoids and carotenoids, such as luteolin. Fig. 3 includes the molecular structure of luteolin, highlighting its characteristic FTIR peaks such as O–H stretching and C=C aromatic ring stretching.

Commercial ZnO and TiO_2 powders were subjected to XRD analysis with the aim of determining their phases, chemical composition, crystal structure and in Fig. 4 as a diffraction image, illustrating the relationship between the intensity and angle values at 2θ. These diffraction peaks provide insight into the phase

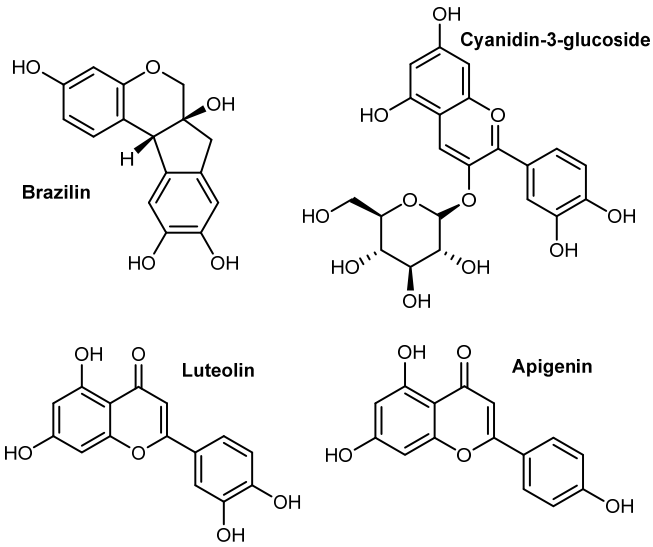

Fig 3. Molecular structure of brazilin, cyanidin-3-glucoside, luteoilin, and apigenin

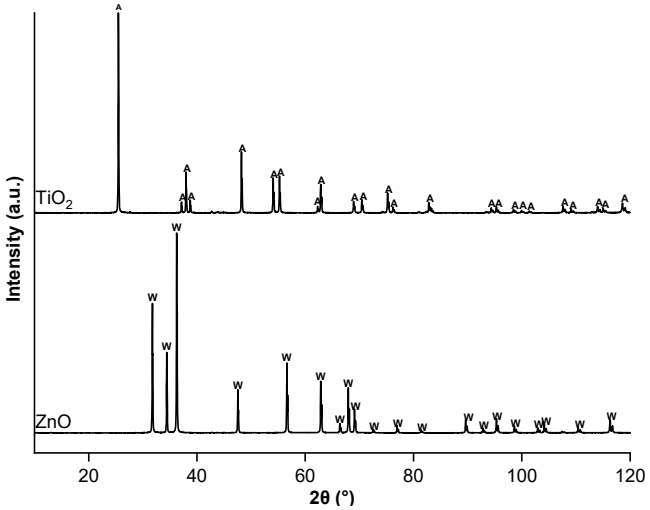

Fig 4. XRD patterns of ZnO and TiO_2 powders

and crystal structure of the material. According to analysis performed using *Match*! software, ZnO diffraction patterns indicate the presence of a wurtzite crystal size. The XRD characterization results are shown phase characterized by a hexagonal crystal structure in the space group *P63mc*. Analytical results also show that the diffraction peaks of TiO_2 correspond to the anatase phase, showing a tetragonal crystal structure in space group *I41/AMD:2*. Table 1 provides details of the fitting results of the XRD data. Based on these results, the estimated crystallite size of ZnO and TiO_2 powder is about 158.1 and 442.6 nm, respectively.

The results of SEM characterization of ZnO and TiO_2 powders are shown in Fig. 5. Morphological examination of ZnO powder shows that the particles resemble wood chips, exhibit inhomogeneity, and tend to agglomerate. In contrast, TiO_2 powder has uniform particles with a spherical shape but also has an agglomeration phenomenon. In particular, the agglomeration of TiO_2 appears more pronounced than that of ZnO, leading to a decrease in the surface area covered by TiO_2 powder. Therefore, this may decrease the available surface energy of the TiO_2 powder [20]. When analyzing the SEM data using *ImageJ*, it is observed that ZnO and TiO_2 powders have a wide range of particle sizes, as shown in Fig. 6. Additionally, using *Origin* to analyze the SEM data shows that ZnO and TiO_2 has a medium particle size vessel with a diameter of about 275 and 190 nm, respectively.

FTIR characterization results of ZnO and TiO_2 powders are shown in Fig. 7. These results were analyzed by contrasting the observed functional groups and wavenumbers. Their respective in ZnO and TiO_2 with existing research. Regarding the analysis of ZnO powder, the wavenumber of 552 cm^{-1} corresponds to the stretching vibration of Zn–O, which is consistent with a study showing the stretching vibration of Zn–O at a wavenumber of 546 cm^{-1}. In addition, the wavenumber 694 cm^{-1} ranges from 608 to 732 cm^{-1} indicating the stretching vibration of ZnO nanoparticles. At the wavenumber of 872 cm^{-1}, which is between 870 and 875 cm^{-1}, there is evidence for the formation of a tetrahedral structure of Zn. The observed 984 cm^{-1} band is consistent with a Zn–O stretching mode for undoped ZnO and is distinct from the elongation effects induced by Mg and Cd doping, as discussed by Kalu et al. [21]. Referring to the Material Safety Data Sheet (MSDS) of ZnO, Mg content is 0.005% and Cd content is 0.0005%. In addition, wavenumbers 1387, 1520, and 1556 cm^{-1} represent C=O stretching, with wavenumber 1561.06 cm^{-1} representing C=O stretching vibration according to Yedurkar et al. research [22]. The wavenumber 2930 cm^{-1}

Table 1. Rietveld-derived crystal size of ZnO and TiO_2 powders using *MAUD* software

Sample	Crystal size (nm)
ZnO	158.1
TiO_2	442.6

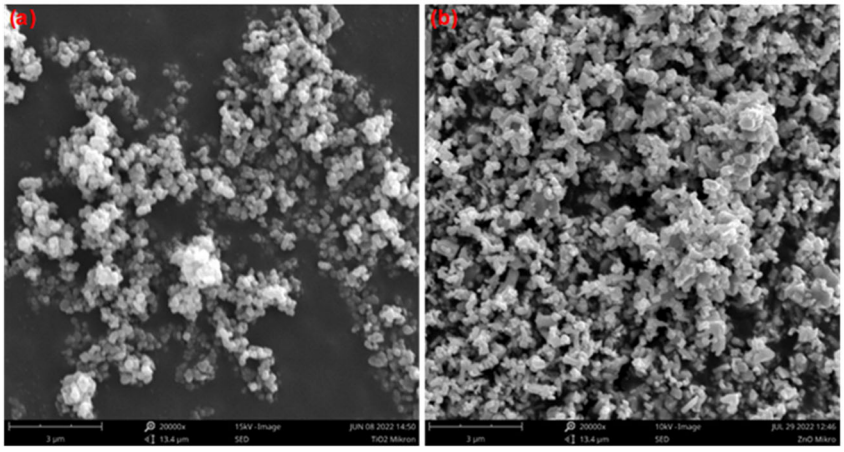

Fig 5. SEM images of (a) ZnO and (b) TiO_2 powders

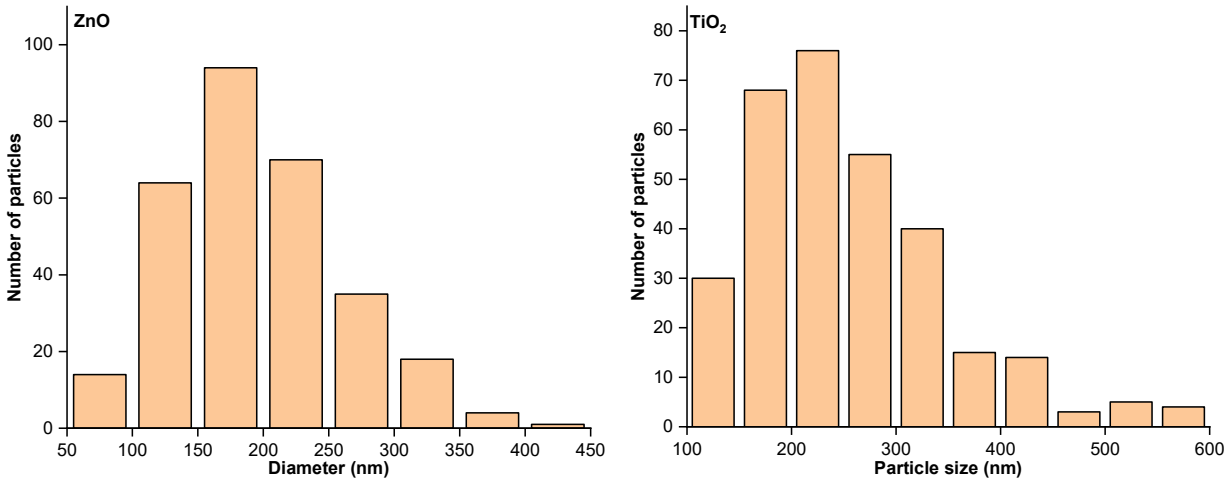

Fig 6. Particle size distribution of ZnO and TiO_2 powders measured by SEM image analysis

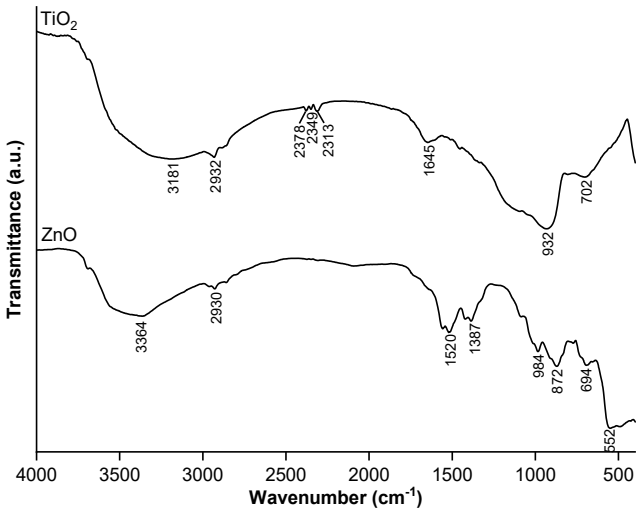

Fig 7. FTIR spectra of ZnO and TiO_2 powders

corresponds to the functional group CH_3, consistent with the study of Vijayalakshmi et al. [23], who determined the vibrational symmetry of the CH_3 group. At 3364 cm^{-1}, there is evidence of relaxation vibrations of O–H functional groups. Regarding the FTIR measurement of TiO_2 powder, the analysis shows Ti–O vibration at 702 cm^{-1}, which according to the study of Kaur et al. [24] links waves in the range 400–900 cm^{-1} to Ti–O. The wavenumber of 932 cm^{-1} can be assigned to the C–O stretching vibration [25-26]. Although the materials used have a purity of 98–99%, there is a possibility that the samples were exposed to organic carbon contaminants (such as CO_2 or other organic substances in the air) during preparation and handling. This contamination could lead to the appearance of C–O, C=O, and CH_3 bands in the FTIR spectra. At 1645 cm^{-1}, there is evidence of O–H stretching and bending, supported by the study of Alosfur et al. [27] associated the wavenumber of 1650 cm^{-1} with the O–H stretching and O–H bending modes related to the physical absorption of water. In addition, the wavenumbers 2313, 2349, and 2378 cm^{-1} represent the O–H groups of the H_2O molecule, consistent with the study of Alosfur et al. [27], correlating the O–H group of water molecules with Ti^{+4} cation. Finally, at 3181 cm^{-1}, in the range 2900–3500 cm^{-1}, there is evidence of O–H group vibrations and Kongsong et al. [28] identified the O–H vibration originating from the Ti–OH at 3443 cm^{-1}.

Moreover, the characterization of ZnO and TiO_2 powders involved employing a UV-vis spectrophotometer to assess their absorbance properties and band gap energy. The UV-vis analysis of ZnO and TiO_2 powders encompassed a wavelength range spanning 200 to 700 nm, as depicted in Fig. 8. Band gap energies for ZnO and TiO_2 were determined using Eq. (1) [29].

$$(h\nu\alpha)^{1/n} = A(h\nu - Eg) \quad (1)$$

The measurement outcomes indicate that ZnO exhibits maximum absorbance peaks at 255 and 345 nm, corresponding to a band gap energy of 3.07 eV. As for TiO_2 powder, its distinctive feature is a maximum absorbance at 325 nm, indicating a band gap energy of 3.17 eV. This band gap energy value closely aligns with the energy value for TiO_2 in the anatase phase, as reported in the previous study [30].

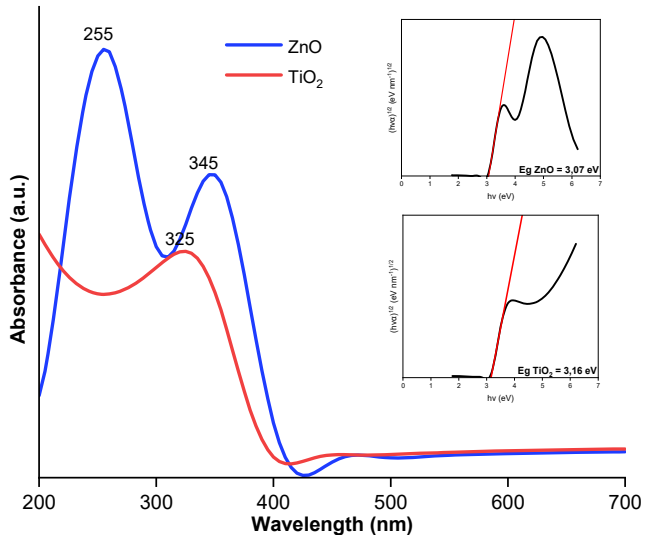

Fig 8. UV-vis absorption spectra and Tauc plot-derived band gap energy of ZnO and TiO_2 powders

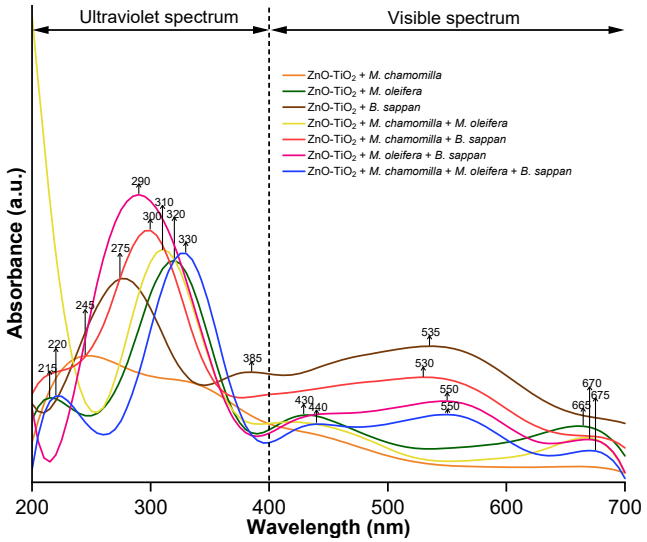

Fig 9. UV-vis absorption spectra of ZnO-TiO_2 films coated with natural dye extract

The ZnO-TiO_2 film was characterized using a UV-vis spectrophotometer to evaluate the absorbance produced by the film. The film was created by coating ZnO-TiO_2 powder with natural dyes, combining variations of one dye, co-sensitized with two dyes and co-sensitized with three dyes. As shown in Fig. 9, the film exhibits a significant absorption peak in the UV range, exhibiting absorption values significantly higher than visible light. In the visible light range, there is a broader absorption peak than that observed in the UV. Mixing one dye with a combination of two or three dyes for co-sensitization aims to achieve panchromatic absorption, thereby maximizing sunlight absorption.

Co-sensitization of *M. chamomilla* and *M. oleifera* resulted in a higher absorption peak than a single dye, as shown in Fig. 10. However, it is important to note that the results of co-sensitization have not yet achieved panchromatic absorption. In the UV light spectrum, when *M. chamomilla* and *B. sappan* are co-sensitized, they exhibit a maximum absorption peak that exceeds the absorption peak of a single dye (Fig. 11). However, it is worth mentioning a co-sensitization of *M. chamomilla* and *B. sappan* that achieves panchromatic absorption, but mainly in the UV area, peaking at 300 nm.

The co-sensitization involving *M. oleifera* and *B. sappan* broadens its absorption in the wavelength range of 200–400 nm, with the absorption peak occurring at 290 nm (Fig. 12). When compared with individual dyes, *M. oleifera* shows a dominant absorption peak in the range of 200–350 nm and *B. sappan* in the range 250–450 nm, the co-sensitization of *M. oleifera* and *B. sappan* shows the ability absorbs a broader spectrum of UV wavelengths, although has slightly lower absorbance values. It should be noted that various factors from natural dye extraction can affect the photovoltaic performance of DSSCs, including extraction temperature,

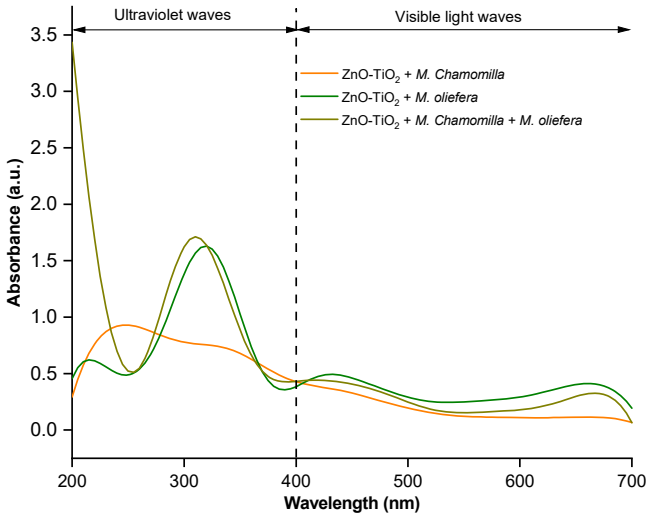

Fig 10. UV-vis absorption spectra of ZnO-TiO_2 films coated with *M. chamomilla* and *M. oleifera* extracts singly and double

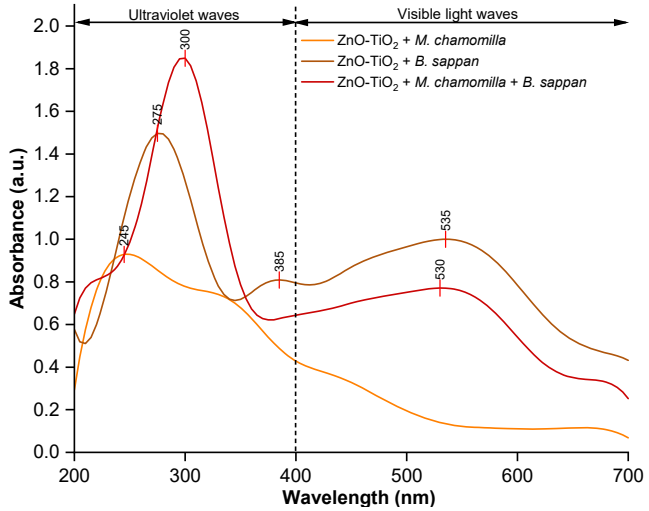

Fig 11. UV-vis absorption spectra of ZnO-TiO_2 films coated with *M. chamomilla* and *B. sappan* extracts singly and double

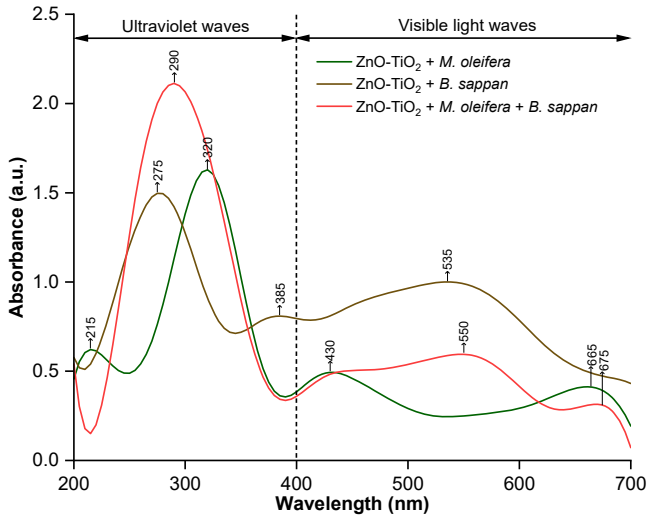

Fig 12. UV-vis absorption spectra of ZnO-TiO_2 films coated with *M. oleifera* and *B. sappan* extracts singly and double

pH of the sensitized solution sensitization, pH immersion time and pigment stability after co-sensitization on the film [31]. The high absorbance value and broad absorption spectrum indicate the ability to capture a larger number of photons, thus potentially improving DSSC performance.

■ CONCLUSION

XRD analysis indicated crystallite sizes of 158 nm for ZnO and 443 nm for TiO_2. The UV absorbance spectrum of ZnO powder showed prominent peaks at 255 and 345 nm, with a band gap energy of 3.07 eV. TiO_2 powder had a peak at 325 nm and a band gap energy of 3.16 eV. FTIR analysis of natural dyes confirmed the presence of functional groups O–H, C–H, C=C and C–O corresponding to chlorophyll, brazilian, apigenin, cyanidin-3-glucoside, and luteolin pigments. The ZnO-TiO_2 films co-sensitized with these dyes showed enhanced UV spectrum peaks. Co-sensitizing with double natural dyes resulted in panchromatic absorption predominantly in the UV spectrum. Despite these promising results, further research is needed to optimize the co-sensitization process and fully understand the limitations of using natural dyes in DSSCs, including their long-term stability and the scalability of the dye extraction process. Future work should also explore the combination of different dye ratios and the potential integration of other semiconductor materials to improve DSSC performance.

■ ACKNOWLEDGMENTS

This research was supported by the Institute for Research and Community Services (LPPM) ITK and the Indonesian Toray Science Foundation (ITSF) through a Science and Technology Research Grant.

■ CONFLICT OF INTEREST

The authors have no relevant financial or non-financial interests to disclose.

■ AUTHOR CONTRIBUTIONS

All authors certify that they have participated sufficiently in the work to take public responsibility for the content.

■ REFERENCES

[1] Abas, N., Kalair, A., and Khan, N., 2015, Review of fossil fuels and future energy technologies, *Futures*, 69, 31–49.

[2] Parisi, M.L., Maranghi, S., and Basosi, R., 2014, The evolution of the dye sensitized solar cells from Grätzel prototype to up-scaled solar applications: A life cycle assessment approach, *Renewable Sustainable Energy Rev.*, 39, 124–138.

[3] Tomar, N., Agrawal, A., Dhaka, V.S., and Surolia, P.K., 2020, Ruthenium complexes-based dye sensitized solar cells: Fundamentals and research trends, *Sol. Energy*, 207, 59–76.

[4] Alhorani, S., Kumar, S., Genwa, M., and Meena, P.L., 2020, Review of latest efficient sensitizer in dye-sensitized solar cells, *AIP Conf. Proc.*, 2265 (1), 03063.

[5] Ansari, A.A., Nazeeruddin, M.K., and Tavakoli, M.M., 2021, Organic-inorganic upconversion nanoparticles hybrid in dye-sensitized solar cells, *Coord. Chem. Rev.*, 436, 213805.

[6] Ramanarayanan, R., Nijisha, P., Niveditha, C.V., and Sindhu, S., 2017, Natural dyes from red amaranth leaves as light-harvesting pigments for dye-sensitized solar cells, *Mater. Res. Bull.*, 90, 156–161.

[7] Angreni, W., Mursal, M., and Yusibani, E., 2018, Sintesa lapisan tipis $MgTiO_3$ dengan metode sol gel, *J. Aceh Phys. Soc.*, 7 (2), 68–84.

[8] Zhang, K., Qiu, L., Tao, J., Zhong, X., Lin, Z., Wang, R., and Liu, Z., 2021, Recovery of gallium from leach solutions of zinc refinery residues by stepwise solvent extraction with N235 and Cyanex 272, *Hydrometallurgy*, 205, 105722.

[9] Nurlaila, R., Musyarofah, M., Muwwaqor, N.F., Triwikantoro, T., Kuswoyo, A., and Pratapa, S., 2017, Phase analysis of ZrO_2-SiO_2 systems synthesized through ball milling mechanical activations, *AIP Conf. Proc.*, 1788 (1), 030122.

[10] Elsandika, G., Putri, A.D.C., Musyarofah, M., and Pratapa, S., 2019, Synthesis of $ZrSiO_4$ powders by a sol-gel method with varied calcination temperatures, *IOP Conf. Ser.: Mater. Sci. Eng.*, 496 (1), 012047.

[11] Musyarofah, M., Astuti, D., Nuraini, I., Azizah, N., Septiana, A.R., Prayitno, B., Husain, H., Yudoyono, G., and Mohamed, Z., 2024, Extraction and optical properties of plant dyes for dye-sensitized solar cell application, *AIP Conf. Proc.*, 2923 (1), 040010.

[12] Buthelezi, N.M.D., Gololo, S.S., and Mugivhisa, L.L., 2022, An assessment of moringa (*Moringa oleifera* L.) seed extract on crop water productivity and physico-biochemical properties of cancer bush (*Sutherlandia frutescens* L.) under deficit irrigation, *Horticulturae*, 8 (10), 938.

[13] Nurlinda, N., Handayani, V., and Rasyid, F.A., 2021, Spectrophotometric determination of total flavonoid content in *Biancaea sappan* (*Caesalpinia sappan* L.) leaves, *JFFI*, 8 (3), 1–4.

[14] Mansour, R., Dhouib, S., and Sakli, F., 2022, UV protection and dyeing properties of wool fabrics dyed with aqueous extracts of madder roots, chamomiles, pomegranate peels, and apple tree branches barks, *J. Nat. Fibers*, 19 (2), 610–620.

[15] Putri, H.F.W., Khusmitha, Q.N., Mahardhika, G.P.C., Hidayati, D.Y.N., Raras, T.Y.M., and Norahmawati, E., 2022, Comparison of phytochemical content and antifungal activity of Bajakah Tampala stem (*Spatholobus littoralis* Hassk.) methanol and ethanol extracts against *Candida albicans*, *Asian J. Health Res.*, 1 (2), 19–24.

[16] Hapsari, S., Yohed, I., Kristianita, R.A., Jadid, N., Aparamarta, H.W., and Gunawan, S., 2022, Phenolic and flavonoid compounds extraction from *Calophyllum inophyllum* leaves, *Arabian J. Chem.*, 15 (3), 103666.

[17] Lai, H.T., Nguyen, G.T., Tran, N.T., Nguyen, T.T., Van Tran, C., Nguyen, D.K., Chang, S.W., Chung, W.J., Nguyen, D.D., Thi, H.P.N., and La, D.D., 2022, Assembled porphyrin nanofiber on the surface of g-C_3N_4 nanomaterials for enhanced photocatalytic degradation of organic dyes, *Catalysts*, 12 (12), 1630.

[18] Yilmaz, C., and Gökmen, V., 2016, "Chlorophyll" in *Encyclopedia of Food and Health*, Academic Press, Oxford, UK, 37–41.

[19] Njoku, D.I., Oguzie, E.E., and Li, Y., 2017, Characterization, electrochemical and theoretical study of the anticorrosion properties of *Moringa oleifera* extract, *J. Mol. Liq.*, 237, 247–256.

[20] Li, R., Chen, G., Dong, G., and Sun, X., 2014, Controllable synthesis of nanostructured TiO_2 by CTAB-assisted hydrothermal route, *New J. Chem.*, 38 (10), 4684–4689.

[21] Kalu, O., Duarte Moller, J.A., and Reyes Rojas, A., 2019, Structural and optical properties of cadmium magnesium zinc oxide (Cd-Mg-ZnO) nanoparticles synthesized by sol–gel method, *Phys. Lett. A*, 383 (10),

1037–1046.

[22] Yedurkar, S., Maurya, C., and Mahanwar, P., 2016, Biosynthesis of zinc oxide nanoparticles using *Ixora coccinea* leaf extract—A green approach, *Open J. Synth. Theory Appl.*, 5 (1), 1–14.

[23] Vijayalakshmi, D., Chellappa, M., Anjaneyulu, U., Manivasagam, G., and Sethu, S., 2016, Influence of coating parameter and sintering atmosphere on the corrosion resistance behavior of electrophoretically deposited composite coatings, *Mater. Manuf. Processes*, 31 (1), 95–106.

[24] Kaur, M., and Verma, N.K., 2014, $CaCO_3/TiO_2$ nanoparticles based dye sensitized solar cell, *J. Mater. Sci. Technol.*, 30 (4), 328–334.

[25] Zarif, M.E., Yehia-Alexe, S.A., Bita, B., Negut, I., Locovei, C., and Groza, A., 2022, Calcium phosphates–chitosan composite layers obtained by combining radio-frequency magnetron sputtering and matrix-assisted pulsed laser evaporation techniques, *Polymers*, 14 (23), 5241.

[26] Soares, L.S., Perim, R.B., de Alvarenga, E.S., Guimarães, L.M., Teixeira, A.V.N.C., Coimbra, J.S.R., and de Oliveira, E.B., 2019, Insights on physicochemical aspects of chitosan dispersion in aqueous solutions of acetic, glycolic, propionic or lactic acid, *Int. J. Biol. Macromol.*, 128, 140–148.

[27] Alosfur, F.K.M., Ouda, A.A., Ridha, N.J., and Abud, S.H., 2019, Structure and optical properties of TiO_2 nanorods prepared using polyol solvothermal method, *AIP Conf. Proc.*, 2144 (1), 030025.

[28] Kongsong, P., Sikong, L., Niyomwas, S., and Rachpech, V., 2014, Photocatalytic antibacterial performance of glass fibers thin film coated with N-doped SnO_2/TiO_2, *Sci. World J.*, 2014 (1), 869706.

[29] Singh, S., and Chakrabarti, P., 2013, Optical characterization of ZnO thin films grown by thermal oxidation of metallic zinc, *Adv. Sci., Eng. Med.*, 5 (7), 677–682.

[30] Kurban, H., Dalkilic, M., Temiz, S., and Kurban, M., 2020, Tailoring the structural properties and electronic structure of anatase, brookite and rutile phase TiO_2 nanoparticles: DFTB calculations, *Comput. Mater. Sci.*, 183, 109843.

[31] Cole, J.M., Pepe, G., Al Bahri, O.K., and Cooper, C.B., 2019, Co-sensitization in dye-sensitized solar cells, *Chem. Rev.*, 119 (12), 7279–7327.